VERTICAL GROUND-WATER MOVEMENT IN SOUTHEASTERN NEW MEXICO AS DETERMINED FROM REGIONAL HEAT-FLOW ESTIMATES

by

David Leigh Jordan

Independent study report
submitted in partial fulfillment
of the requirements for the degree of
Master of Science in Geophysics

May 1989

NEW MEXICO INSTITUTE OF MINING AND TECHNOLOGY
SOCORRO, NEW MEXICO

I. INTRODUCTION

Ground water in large sedimentary basins usually moves very slowly, and it is difficult to observe this movement directly. Instead, we can study indirect parameters that are affected by ground-water flow, such as heat flow. Heat-flow studies in sedimentary basins can provide valuable insight into regional ground-water flow regimes. Ground-water flow can significantly alter the heat flow in a sedimentary basin from the purely conductive regime that would be expected if there were no water flow.

In a general sense, one would expect depressed surface heat flow in recharge areas and elevated surface heat flow in discharge areas. Recharge areas are characterized by zones where there is a significant component of downward ground-water flow, while discharge areas are characterized by zones of predominantly upward ground-water flow. Water flowing downward will carry heat with it, away from the surface, thus creating an area of depressed surface heat flow. Likewise, water that has been heated at depth and flows upward will bring heat nearer to the surface, thus elevating the surface heat flow. Kilty and Chapman (1980), and Garvin and Freeze (1984), among others, present results of numerical models which support this theory. Smith and Chapman (1983) include a thorough literature review of recent work on surface heat-flow perturbations caused by ground-water flow.

Another way to envision the influence of vertical ground-water flow on heat-flow data is to appreciate the effect that vertical ground-water flow has on the temperature data. In the present study we generally make shallow and deep estimates of heat flow. The shallow heat-flow estimates are based on temperature gradients between the surface and relatively shallow temperatures. The deep heat-flow estimates are based on gradients between shallow and deep temperature measurements. Upward ground-water flow from deep depths will generally raise the shallow temperatures, therefore increasing the shallower temperature gradients and consequently shallow heat flows. Because of the elevated shallow temperatures, the deep gradients, and hence deep heat flows, will be

lowered. On the other hand, downward ground-water flow from shallow depths will decrease the shallow temperatures, therefore decreasing shallow temperature gradients and shallow heat flows. Because the shallow temperatures are lowered and the deep temperatures remain the same, the deep gradients will be increased, as will the deep heat flows.

In this study, we examine the variation of heat flow with depth along several profiles in southeast New Mexico. We divide heat-flow data into two groups : shallow heat flows and deep heat flows. The shallow heat flows show areas of surface ground-water recharge and discharge. As mentioned above, shallow heat flows are also affected by deep vertical ground-water movement. This effect is especially pronounced in the area west of the Pecos river, where there is a significant component of recharge to the San Andres formation from deeper formations, and thus deep vertical ground-water movement.

II. BRIEF DESCRIPTION OF THE STUDY AREA

The study area is located in southeast New Mexico and encompasses most of the Northwest Shelf of the Delaware Basin (Figure 1). This is the region of the Permian Basin north of the Capitan Reef Front. The study area is bounded on the southwest by the Gaudalupe mountains, on the west by the Sacramento mountains, and on the north by the Matador Arch. The Pecos river valley runs approximately north-south through the middle of the study area. The surface topography west of the Pecos river slopes eastward from the base of the mountains to the river. Elevations range from about 1525 meters at the base of the Sacramento and Gaudalupe mountains, to slightly less than 1070 meters at the Pecos river. East of the Pecos river, the topography rises abruptly along the Mescalero Ridge to the Southern High Plains (about 1220 meters), which dip gently eastward into Texas. The climate of the study area is semi-arid, with short winters and long, hot summers. Most of the precipitation to the area falls from May to September in localized thunderstorms. Winter snows accumulate in the high mountains and enter the Pecos river

valley as spring runoff.

III. TEMPERATURE DATA

The temperature data used were uncorrected bottom-hole temperatures taken from oil well log headers. Each data point consisted of a temperature at a given depth. The data were grouped by township (an approximately 9.7 km by 9.7 km area), and were then divided into two categories : shallow and deep points. The shallow temperatures generally clustered around 1000 meter depths, while the deep temperatures clustered near 3000 meters.

In order to calculate surface temperatures, a plot of average yearly temperature (as determined from Gaben and Lesperance, 1977) versus elevation across the study area was made. A least mean squares line was then fit to the data to obtain a function which gave surface temperature for corresponding elevation. The surface temperature of a township was calculated from the average elevation of the township. Elevation variations across any one township were only a few percent, so the average elevation is a good approximation within a township.

Temperature data were taken along two profiles (Profile 1 and Profile 2, Figure 2). Profile 1 incorporates 15 townships, profile 2 includes 12 townships. There are 784 bottom-hole temperatures along Profile 1, and 1291 BHTs along Profile 2. The data in each township were grouped to yield estimates of shallow and deep heat flow. Shallow gradients were calculated by fitting a least mean squares straight line from the surface temperatures to the shallow temperature-depth points. Deep gradients were calculated by fitting a least mean squares straight line from the shallow temperature-depth points to the deep points (Figure 3). The slopes of these lines were taken to be the shallow and deep temperature gradients, respectively, of each township. The data were grouped this way in order to smooth random variations associated with BHT measurements. Since the stratigraphy in the Delaware Basin is fairly continuous laterally , we assumed that the lithology,

thickness, and spatial position of the various formations will vary little across one township.

It is also important to consider corrections to the bottom-hole temperature data. The actual formation temperature will be perturbed by the drilling operation. This perturbation will be a function of many parameters such as depth, time of drilling, and physical properties of the formation and drilling fluid (Carstens and Finstad, 1981; Chapman, et al, 1984; Dowdle and Cobb, 1975; Lee, 1982). Bottom-hole temperatures will generally be lower than actual formation temperatures, since the formation will have been cooled by drilling fluids. Deeper formation temperatures (to about 3000 meters) are more perturbed by cool drilling fluids than are shallower formation temperatures, because the temperature differential between the drilling fluid and the formation is greater at deeper depths.

If several temperatures at a given depth are available at increasing times since circulation, the Horner plot reasonably estimates the formation temperature (Fertl and Wichmann, 1977). However, such data are uncommon in the present study area. Therefore we chose to apply the AAPG correction to the BHT data (derived by Kehle (1971) for Gulf Coast sediments and given in Bebout, et al, 1978). Although the AAPG correction was not derived for our study area, it is an appropriate correction to consider in order to obtain insight into the errors involved with the BHT data. Since variations in heat flow with depth are of concern, the AAPG correction will afford an opportunity to appreciate uncertainties in shallow and deep heat-flow estimates which may be associated with using uncorrected BHT data. We will discuss the significance of the AAPG correction below when we consider the results of the study.

IV. THERMAL CONDUCTIVITY DATA

Given a constant basement heat flux and no ground-water flow, variations in the geothermal gradient can be caused simply by variations in thermal conductivity. How-

ever, variations in heat flow can often be attributed to variations in the thermal gradient only. In a sedimentary basin where structure and lithology are rather laterally continuous, conductivities would not be expected to vary greatly across the basin. Thus if the thermal conductivities are measured and found not to vary laterally, then variations in the geothermal gradient can be attributed to ground-water movement, assuming that there is no variation in mantle heat sources or crustal radiogenics.

Thermal conductivities were measured on drill cuttings from five wells across the study area (Figure 2). Measurements were performed using the method described by Reiter and Hartman (1971). We made 162 rock matrix thermal conductivity measurements, typically about 30 per well. Well depths ranged from 2876 to 4051 meters. Sampling intervals were generally 120 meters, but were reduced in areas of rapidly varying lithology. The rock matrix thermal conductivity of a given formation or group of formations was taken to be the harmonic mean of the matrix thermal conductivities of all intervals measured within the formation or group of formations. Matrix thermal conductivities were corrected for porosity using the relation

$$k_r = k_w^{\phi} k_m^{1-\phi} \qquad (1)$$

where k_r is the actual rock thermal conductivity, k_w is the conductivity of water, k_m is the rock matrix conductivity, and ϕ is the porosity of the rock (Sass, et al, 1971). Porosities were estimated for each formation or group of formations from porosity logs and laboratory measurements, and we initially assumed that the porosity did not vary laterally. Porosity-corrected thermal conductivities are given in Table 1. Note that there are significant lateral variations in thermal conductivity, especially in the Abo and younger formations. The general trend is conductivity decreasing eastward in the study area from range 27E to 35E, as can be seen from the values of whole-well thermal conductivity.

Rather than assuming constant lateral porosity, we might consider that in the San Andres formation, for example, the porosity west of the Pecos river is quite high,

perhaps 20%, while the porosity decreases significantly east of the river, to perhaps 5%. Unfortunately, no measured values are available, to our knowledge. However, most of the water in the San Andres formation is thought to flow through solution cavities (Morgan, 1941; Fiedler and Nye, 1933), and we assume that in a macroscopic sense, this secondary porosity is evenly distributed. High porosity will tend to lower thermal conductivity, since the conductivity of water is lower than the conductivity of most rocks. A few simple calculations using a first-order model where the porosity in the San Andres formation decreases linearly from 20% to 5% along Profile 1 show that such a porosity variation would dampen the decreasing thermal conductivity trend (Figure 4a). Therefore we propose that the effect of decreasing thermal conductivity may be effectively counteracted by the trend in porosity, and that indeed, the thermal conductivity across the basin remains fairly constant.

In Figure 4b we present results of heat-flow calculations using both least mean squares line fit conductivities (Figure 4a), and mean conductivities along Profile 1. It is apparent that although the magnitude of the heat-flow anomalies change somewhat, the character of the major heat-flow trends remains the same. Therefore by assuming mean conductivities for each formation or group of formations we will not affect the first-order results of the study.

V. HYDROGEOLOGY

A schematic hydrogeologic cross-section is shown in Figure 5. The cross-section is based on the literature, as well as heat-flow results. The ground-water flow in the study area can generally be divided into shallow and deep flow systems. Regional flow in both systems is topography-controlled. West of the river, the shallow flow conduit is primarily the San Andres formation (Permian age). The ground water in the San Andres carbonate aquifer flows generally to the east and southeast, until it reaches the Pecos river. The San Andres is confined and artesian in the area of the Pecos river. Much of the

water in the San Andres discharges to the river by percolating upward in a high-porosity zone developed in the vicinity of the river (Morgan, 1941). Previous studies (Summers, 1981) as well as the present study, present evidence for downward flow at depth in the area of the Pecos river. East of the river, shallow ground-water flow is in the shallow high plains aquifer. The shallow high plains aquifer includes the Dockum Group (Triassic age) and the overlying Ogallala formation (Tertiary age). The ground water in these aquifers flows generally to the east (Ash, 1963), down the regional slope of the beds. There is a shallow ground-water divide generally coincident with the Mescalero Ridge (Summers, 1981; Dutton and Orr, 1986). East of the divide, flow in the shallow high plains aquifer is eastward; to the west flow is discharging to the Pecos river.

Recharge to the shallow flow system is primarily by surface precipitation. The San Andres formation is recharged along its karstic outcrop surface, where it is unconfined west of range 23E. The San Andres formation is also thought to get some component of deep recharge from the underlying Yeso and Abo formations (Gross and Hoy, 1980; Fiedler and Nye, 1933). The Abo and Yeso formations are recharged in the Sacramento Mountains to the west. Recharge to the eastern high plains occurs mainly from precipitation onto the outcrop of the Ogallala formation. The downward flow from the Ogallala to the Dockum is probably minimal (Havenor, 1968). Ground water in the Dockum is isotopically different from water found in the overlying Ogallala (Dutton and Simpkins, 1986), so there is little evidence for vertical mixing. However, there is probably some downward flow from the Ogallala formation to the Dockum Group where they are hydraulically connected, since the water table in the Ogallala formation is higher than the head in the Dockum (Summers, 1981; Dutton and Simpkins, 1986).

The deep flow system consists of the Permian Wolfcamp carbonates and underlying Pennsylvanian through Ordovician carbonates and shales. The saline waters in the deep aquifer flow generally northeastward (McNeal, 1964). Kaiser (1985) suggests that the presence of meteoric water in the deep flow system indicates recharge from the Sacra-

mento mountains to the west.

East of range 23E, the shallow and deep flow systems are separated by an evaporite aquitard, which thickens to the east (Figure 5). In the area of the Pecos river the San Andres is confined by the Artesia Group (Permian age). Farther east of the river, the Ochoa Series (Permian age), as well as the Artesia Group form an evaporite aquitard, and act to separate the shallow high plains flow system from the deeper flow system (Senger and Fogg, 1987). The western boundary of the evaporite aquitard is unknown, as is its exact geometry. However, the existence of the Pecos river indicates some lateral and vertical porosity change which is associated with upward ground-water flow to the surface. East of the Pecos the porosity of the San Andres decreases, due to an increased evaporite content. The Yeso and Abo formations also become significantly more evaporitic east of the Pecos river (King, 1942), and are included in the evaporite aquitard. West of the Pecos river, the shallow and deep flow systems are not really separated from each other, and flow is mainly lateral and eastward-southeastward throughout the entire sequence of strata. However, previous studies, as well as the present one, indicate some component of recharge from the Yeso and Abo formations into the San Andres, and therefore indicate some upward vertical flow.

Examination of equivalent freshwater heads calculated from drill stem test pressures (McNeal, 1964) in the study area indicates that the deep basin flow system east of the Pecos river may be underpressured. However, the waters in the shallow flow system are typically much less saline than the deep basin brines, and it is difficult to delineate vertical flow using equivalent freshwater heads when the density of the fluids is variable (Blair, 1987). An underpressured deep basin would be associated with flow downward from the shallow high plains aquifers, through the evaporite aquitard, and into the deep basin, similar to the situation observed in the Palo Duro Basin to the north (Senger and Fogg, 1987). Summers (1981) also suggests downward flow across the evaporite aquitard, in the area around Carlsbad caverns.

V. ERROR ANALYSIS

Error bars represent unsystematic uncertainties estimated by considering the standard deviation of the mean of the thermal conductivity data and the standard deviations for the temperature gradients in each township. We used the average of the standard deviation of the mean of the whole-well thermal conductivity as a measure of the average uncertainty of the thermal conductivity over the whole study area. Our heat-flow error bars were computed by the method of Young (1962), given by

$$\sigma_{hf}^2 = \frac{dT^2}{dz}\sigma_k^2 + k^2\sigma_{\frac{dT}{dz}}^2 \qquad (2)$$

where σ_{hf} is the uncertainty of the heat-flow estimate, σ_k is the average of the standard deviation of the mean of the whole-well thermal conductivity, and $\sigma_{\frac{dT}{dz}}$ is the standard deviation of the temperature gradient. Gradients and errors are given Table 2 and Table 3.

We should also compare the heat-flow profiles after the AAPG correction has been applied to the temperature data. Corrected heat flows are given in Table 4 and Table 5. In comparing the corrected Profile 1 (Figure 7) with the uncorrected Profile 1 (Figure 6) we see that although the magnitudes of the heat flows differ, the character of the uncorrected and corrected profiles is quite similar. Since our temperature measurements are increasingly underestimated with depth due to the cooling of the formation by drilling fluids, we might expect the corrected gradients and heat flows to be greater, as they are (Figure 7). The main differences between the corrected and uncorrected profiles is the magnitude of the differences between the shallow and deep heat flows. For example, the difference between the shallow and deep heat flows along Profile 1 in the vicinity of the Pecos river is about 16 mW/m2 on the uncorrected profile and 26 mW/m2 on the cor-

rected profile. The average heat flow for the corrected Profile 1 of 50 mW/m2 seems a perfectly reasonable value for background heat flow and agrees well with published values (Herrin and Clark, 1956). In fact, 50 mW/m2 is probably a more representative value than 36 mW/m2, the approximate average heat flow along the uncorrected profile.

VI. RESULTS

In Figure 8 we present a simple conceptual model to explain the effects of vertical ground-water flow on temperatures and heat flows. Upward flow of warm ground water, as long as it comes from below where the shallow points are measured, will increase the shallow temperatures, and hence shallow gradients and heat flows. The increase in shallow temperatures will lower the deep gradient, even if the deep temperatures stay the same. Downward ground-water flow, from below where the shallow points are measured, should tend to decrease deep temperatures. Lowering the deep temperatures would tend to lower the gradient, and thus the heat flow. Therefore we see that a depressed deep heat flow could be caused by both upward ground-water flow from below the shallow points, as well as downward flow from above the deep points.

Uncorrected heat flows and errors are given in Table 6 and Table 7. Uncorrected heat flows along both profiles are shown in Figure 6. The profiles were plotted using a three-point averaging technique to smooth the data. Along both profiles, it appears that the shallow and deep heat flows generally mirror each other about the same average value (the mean value for all data in each profile is about 36 mW/m2). Note that in the western portion of both profiles, we see an elevated shallow heat flow and a lowered deep heat flow. In this area, there is upward flow discharging to the Pecos river. In order to create an elevated shallow heat flow, some water must be flowing upward from depths below our shallow temperature points, bringing heat with it. The idea that the shallow aquifer gets some component of deep recharge has also been suggested by Gross and Hoy (1980), and Fiedler and Nye (1933). Note also that the highest shallow heat flow

values in both Profile 1 and Profile 2 coincide with the Pecos river. Note that Profile 1 is much broader than Profile 2, probably in part because it bisects the regional heat-flow anomaly at an oblique angle (see Figure 9).

Along Profile 1 (Figure 6), the shallow heat flow decreases with distance eastward from the Pecos river, and the deep heat flow generally increases. This observation indicates that the amount of upward ground-water movement decreases eastward from the Pecos river. Note that the difference between the magnitude of the shallow and deep heat flow is probably a qualitative indication of the amount and/or scale of vertical ground-water movement. By using the term scale we refer to the vertical extent of vertical ground-water flow. In the far eastern portion of the profile the shallow and deep heat flows converge to a regional average of about 36 mW/m2, while the shallow values remain about 4 mW/m2 higher than the deep values. Although this observation may suggest that there is still some slight upward ground-water movement in the eastern regions of the profile, any upward flow would be considerably less than near the Pecos river, and may well be nonexistent, considering the overlapping error bars.

Along Profile 2 (Figure 6), we also see a marked decrease in the shallow heat flow eastward from the Pecos river, along with an increase in the deep heat flow. Again, this is probably due to a decrease in the amount of upward vertical ground-water flow. The deep heat flow becomes somewhat higher than the shallow heat flow east of about range 31E. Areas where the deep heat flow is greater than the shallow heat flow are probably areas of relatively shallow downward vertical ground-water flow. We might therefore expect some amount of downward flow east of about range 31E. Although once again overlapping error bars make such conclusions uncertain. Vertical ground-water flow may occur downward from the high plains aquifer through the evaporite aquitard, and into the underpressured deep basin flow system (Senger and Fogg, 1987). The magnitude of any downward ground-water flow along the eastern half of the profile is probably much less than that of the upward ground water flow in the area around the Pecos river,

since the difference between the shallow and deep heat flows is small and uncertain.

In areas of lateral water movement the heat flow should not change significantly with depth, thus when the deep and shallow heat flows have similar values any water flow should be nearly lateral. On Profile 2 (Figure 6), the deep heat flow is only slightly higher than the shallow heat flow east of about range 31E, so although there may be a small component of downward water movement in the area, most of the flow is probably lateral. Alternatively, on Profile 1 (Figure 6), the deep heat flow remains only slightly lower than the shallow heat flow eastward from the Pecos river. This also indicates mainly lateral water flow, with perhaps a slightly upward component.

Different directions of vertical ground-water flow are suggested by the eastern portions of Profile 1 and Profile 2 (Figure 6), although overlapping error bars require such suggestions to be uncertain. This difference in vertical flow may possibly be explained by the difference in the geology of the two areas. At the eastern end of Profile 1, there is a major thinning of the deep basinal sediments and shallowing of the basement due to the presence of the Matador Arch (Figure 1). Because the deep basinal sediments pinch out over the Matador Arch, the deep-basin flow system becomes severely confined. It is quite possible that conditions responsible for downward ground-water flow along Profile 2 do not exist along Profile 1.

From Figure 7 we see that on the corrected Profile 2 the shallow and deep heat-flow values do not cross over, as in the uncorrected Profile 2 (Figure 6). Previously we assumed that the crossover of the heat-flow values indicated a transition from upward to downward flow; and this conclusion is consistent with hydrogeologic evidence. However, the corrected data (Figure 7) do not support this. Consequently we cannot be sure if the crossover of the uncorrected data (Figure 6) is merely a product of the uncorrected data, or if the lack of a crossover in the corrected data relates to a fundamental error in applying the AAPG correction to the present study area. Again overlap of errors makes uncertain any conclusion about upward or downward ground-water flow. In either case

the vertical water flow here is considerably less than near the Pecos river.

It is also informative to note the change in heat flow along both profiles, when that heat flow is measured from the surface to the deep points (leaving out the shallow points). In Figures 10 and 11, we see that these heat flows are lowered in the area of the Pecos river. Thus we have reason to suspect that there is significant downward ground-water flow in this area, which decreases deep temperatures, and hence surface-to-deep heat flows. Downward flow, caused by the presence of the evaporite aquitard (Figure 5), seems quite reasonable. Thus in addition to an increase in the shallow temperatures, we are observing a decrease in the deep temperatures, probably caused by downward flow around the evaporite aquitard.

VII. NUMERICAL MODELING

A two-dimensional finite-difference model was used to simulate ground-water flow and heat transfer. The numerical model consisted of two modules. The first module solves the two-dimensional equation describing steady-state ground-water flow, given by

$$\frac{\partial}{\partial x}\left(K_x \frac{\partial h}{\partial x}\right) + \frac{\partial}{\partial z}\left(K_z \frac{\partial h}{\partial z}\right) = 0 \qquad (3)$$

where K_x and K_z are hydraulic conductivity in the x and z directions, respectively. After the head distribution and Darcy velocities in the model have been computed, the second module is used to solve for the temperature distribution. The two-dimensional equation for steady-state conduction and convection in a porous medium is given by

$$\varrho_f c_{p_f}\left(q_x \frac{\partial T}{\partial x} + q_z \frac{\partial T}{\partial z}\right) - k_r\left(\frac{\partial^2 T}{\partial x^2} + \frac{\partial^2 T}{\partial z^2}\right) = 0 \qquad (4)$$

where ϱ_f is the fluid density, c_{p_f} is the specific heat of water, k_r is the thermal conductivity of the water-rock matrix, and q is the Darcy flux. We assume that the ground-water

flow system is steady state, that the density of the water remains constant, and that the water–rock matrix thermal conductivity remains constant throughout the basin. A more complete description of the numerical model, including sensitivity analysis, can be found in Barroll (1989, in prep).

The model was constructed to be coincident with Profile 2, because Profile 2 is the more representative two–dimensional cross–section of the heat–flow anomaly (Figure 12). Hydrologic properties of rocks in the study area are based on values given in Senger and Fogg (1987), for similar rock types in the Palo Duro Basin. Values from Rehfeldt and Gross (1982) were also used in representing the evaporite aquitard. A constant head is prescribed on both the left and right boundaries of the model. On the right boundary of the model, the representative head level is assumed to be that of the Dockum Group, and values are taken from Dutton and Simpkins (1986). Flow in the overlying Ogallala is significant, but is probably somewhat isolated from the flow in the Dockum, which we assume is part of the regional system. At the surface of the model, the head is prescribed from the left boundary to the Mescalero Ridge. Head values are assumed to be generally coincident with topography. From the Mescalero Ridge to the right–hand boundary of the model a constant no–flow boundary is prescribed. There may be recharge in this area, but we assume that the amounts are relatively small. The bottom boundary is a no–flow boundary.

VIII. LIMITATIONS OF THE NUMERICAL MODEL

There are various limitations inherent in the numerical model. We have represented a very complex regional hydrologic system in a rather simplistic manner. It is difficult for one cross–section through the basin to adequately represent flow in both the deep and shallow flow systems; the flow in the shallow system is to the southeast, while flow in the deep basin is to the northeast. The estimates of hydraulic properties are not

well constrained. They are based on published values, known hydrogeologic features, and a process of fitting the model results to field-derived data. The geometry of the evaporite aquitard, a very important regional hydrogeologic feature, is not well known, nor are its hydrologic properties.

The porosity, which may have a large local effect both on thermal and hydraulic conductivity, is not well known. The model does not take into account the varying properties of water as a function of temperature and salinity, both of which probably vary within the basin. Temperature increases with depth in the basin, which will tend to lower the density and viscosity of water and in turn alter it hydrologic properties. Salinity increases with depth, tending to increase density and viscosity of water. These two processes may, in part, counteract each other.

Nevertheless, the numerical model contains the essential, regional features of the hydrologic system. Namely, the Pecos river, the High Plains, the evaporite aquitard, and the shallow and deep flow systems. A possible check on the hydrogeologic model is the mass flux in the Pecos river valley, which is fairly well known (Rehfeldt and Gross, 1982). We discuss results of such calculations in the next section.

IX. NUMERICAL MODELING RESULTS

Representative model results are shown in Figure 13 and Figure 14. In some ways, they are similar to the results from the field-derived data, but they are also lacking. Note that a strong peak in the shallow heat flow (Figure 13), as well as elevated temperatures (Figure 14), coincide with upward ground-water movement near the Pecos river. The magnitude of the peak is quite consistent with our AAPG-corrected heat-flow values (Figure 7). However, the width of the peak that we see in the model results is not nearly as broad as in the field results. This may be due to the fact that in the model, the water flowing upward near the Pecos river is doing so over a short lateral distance, whereas in actuality, upward ground-water flow to the Pecos river probably occurs over a large lat-

eral distance. We might explain this geologically by hypothesizing that the evaporite aquitard is somewhat discontinuous, allowing many vertical paths to the surface for the water to follow.

Mass fluxes in the model do not match well with published values. The model mass flux across the Pecos river valley is about 10^{-6} m2/sec, while Rehfeldt and Gross (1982) give a value of approximately 10^{-9} m2/sec (approximately along our Profile 2). Again, this indicates that there is probably less lateral flow across the model basin than there should be. With greater lateral flow, less of the total mass flux in the system would be flowing upward to the top of the model. However, less upward ground-water flow may decrease the magnitude of the shallow heat-flow anomaly.

Deep heat flows in the model results do not generally match field-derived results. However, as can be seen from Figure 13, decreased deep heat flows do seem to be coincident with downward ground-water flow. In the model results we do not see the very low deep heat flows near the Pecos river, probably because the model fails to reproduce the amounts of downward ground-water flow below the Pecos river that we expect.

X. CONCLUSIONS

We have shown that regional heat flow can be significantly altered by vertical ground-water movement, such as in the area near the Pecos river in southeastern New Mexico. Shallow, upward discharge to the Pecos river significantly increases shallow heat flows in that area. We also see evidence of downward flow at depth in the area of the Pecos river (from surface-to-deep heat-flow data). This conclusion agrees with Summers (1981), who also predicted downward flow around the evaporite aquitard, and into the deep basin.

It is important to note that the effects of ground-water flow seen in the heat-flow data will be a function of the depth of the temperature data. Upward ground-water

flow will only affect shallow heat flow if it comes from depths below the shallow temperature measurements. Deep heat flows will be decreased by downward water flow only if it comes from depths above the deep temperature measurements. Thus we are able to see differences in vertical ground-water flow as a function of depth, by examining heat flows at different depths.

Numerical modeling results reproduced qualitatively some the observed heat-flow phenomena caused by vertical ground-water flow. However, more work is needed. One obvious possibility is to use a finer finite-difference grid. Unfortunately this presents problems due to the very large horizontal to vertical dimension ratio of the study area. Thus if square grid blocks are used in the model, and there is a great amount of detail in the vertical direction, there will be an unreasonably large number of grid blocks in the horizontal direction, and hence very long computing times will be necessary.

REFERENCES

Ash, S., Ground water in northern Lea county, New Mexico, Hydrologic Investigations Atlas HA-62, USGS, 1963.

Barroll, M., Unpublished Ph.D. thesis, New Mexico Institute of Mining and Technology, 1989.

Bebout, D. G., R. G. Loucks, and A. R. Gregory, Frio sandstone reservoirs in the deep subsurface along the Texas gulf coast : their potential for production of geopressured geothermal energy, Texas Bureau of Economic Geology Report of Investigations no. 91, 1978.

Blair, E. S., Analysis of hydraulic gradients across the host rock at the proposed Texas panhandle nuclear-waste repository site, Ground Water, vol. 25, no. 4, p440-447, 1987.

Bredehoeft, J. D., W. Back, and B. B. Hanshaw, Regional ground-water flow concepts in the United States : historical perspective *in* T. N. Narasimhan, ed., Recent Trends in Hydrology, Geological Society of America special Paper 189, p297-316, 1982.

Chapman, D. S., T. H. Keho, M. S. Bauer and M. D. Picard, Heat flow in the Uinta Basin determined from bottom hole temperature (BHT) data, Geophysics, vol. 49, no. 4, p453-466, 1984.

Carstens, H. and K. G. Finstad, Geothermal gradients of the Northern North Sea Basin, 59-62 degrees north, *in* Illing, L. V. and G. D. Hobson, eds., Petroleum geology of the continental shelf of northern Europe, p152-161, 1981.

Dowdle, W. L. and W. M. Cobb, Static formation temperature from well logs : an empirical method, Journal of Petroleum Technology, vol. 184, no. 1, p1326–1330, 1970.

Dutton, A. R., and E. D. Orr, Hydrology and Hydrochemical Facies of the San Andres formation in Eastern New Mexico and the Texas Panhandle, Report of Investigations No. 157, Texas Bureau of Economic Geology, 1986.

Dutton, A. R. and W. W. Simpkins, Hydrogeochemistry and water resources of the Triassic Lower Dockum Group in the Texas Panhandle and eastern New Mexico, Report of Investigations No. 161, Texas Bureau of Economic Geology, 1986.

Fertl, W. H. and P. A. Wichmann, How to determine static BHT from well log data, World Oil, vol. 27, no. 11, p105–106, 1977.

Foster, R. W. and T. F. Stipp, Preliminary geologic and relief map of the Precambrian rocks of New Mexico, Circular 57, New Mexico Bureau of Mines and Mineral Resources, 1961.

Gaben, V. L. and L. E. Lesperance, New Mexico Climatological Data : Precipitation, Temperature, Evaporation, and Wind; Monthly and Annual Means, W. K. Summers and Associates, Socorro, New Mexico, 436 p, 1977.

Garven, G. and R. A. Freeze, Theoretical analysis of the role of ground water flow in the genesis of stratabound ore deposits, American Journal of Science, vol. 284, p1085–1124, 1984.

Gross, G. W. and R. N. Hoy, A geochemical and hydrologic investigation of ground-water recharge in the Roswell Basin of New Mexico : summary of results and updated listing of tritium determinations, New Mexico Water Resources Research Report No. 122, 1980.

Havenor, K. C. , Structure, stratigraphy, and hydrogeology of the northern Roswell artesian Basin, Chaves County, New Mexico, Circular 93, New Mexico Bureau of Mines and Mineral Resources, 1968.

Havens, J. S., Recharge studies on the High Plains in northern Lea County, New Mexico, USGS Water Supply Paper 1819-F, 1966.

Herrin, E. and S. P. Clark, Jr., Heat flow in west Texas and eastern New Mexico, Geophysics, vol. 21, no. 4, p1087-1099, 1956.

Kaiser, W. R., Cross-formational flow in the Palo Duro Basin : Texas panhandle, Texas Bureau of Economic Geology Open File Report WTWI-1985-33, 1985.

Kilty, K, and D. S. Chapman, Convective heat transfer in selected geologic situations, Ground Water, vol. 18, no. 4, p386-394, 1980.

King, P. B., Permian of West Texas and southeastern New Mexico, AAPG Bulletin, vol. 26, p535-6763, 1942.

Lee, T. C., Estimation of formation temperature and thermal property from dissipation of heat generated by drilling, Geophysics, vol. 47, no. 11, p1577-1584, 1982.

Morgan, A. M., Depth of active solution by ground waters in the Pecos Valley New Mex-

ico, Transactions American Geophysical Union, vol. 22, p779–783, 1941.

Rehfeldt, K. R., and G. W. Gross, The carbonate aquifer of the central Roswell Basin : recharge estimation by numerical modeling, New Mexico Water Resources Research Institute Report No. 142, 1982.

Reiter, M. and H. Hartman, A new steady–state method for determining thermal conductivity, Journal of Geophysical Research, vol. 76, no. 29, p7047–7051, 1971.

Sass, J. H., A. H. Lachenbruch, and R. J. Munroe, Thermal conductivity of rocks from measurements on fragments and its application to heat–flow determinations, Journal of Geophysical Research, vol. 76, no. 14, p3391–3401, 1971.

Senger, R. K. and G. E. Fogg, Regional underpressuring in deep brine aquifers, Palo Duro Basin, Texas : 1. Effects of hydrostratigraphy and topography, Water Resources Research, vol. 23, no. 8, p1481–1493, 1987.

Smith, L. and D. S. Chapman, On the thermal effect of ground–water flow : 1. Regional scale systems, Journal of Geophysical Research, vol. 88, no. 131, p593–608, 1983.

Stratigraphic Research Committee, West–east correlation section San Andres mountains to New Mexico–Texas line : southeast New Mexico, Roswell Geological Society, 1956.

Summers, W. K., Ground–water head distribution in the third dimension of the Pecos River Basin, New Mexico, New Mexico Geology, vol. 3, no. 1, p6–9, 1981.

Young, H. D., Statistical treatment of experimental data, McGraw-Hill, New York, 172p, 1962.

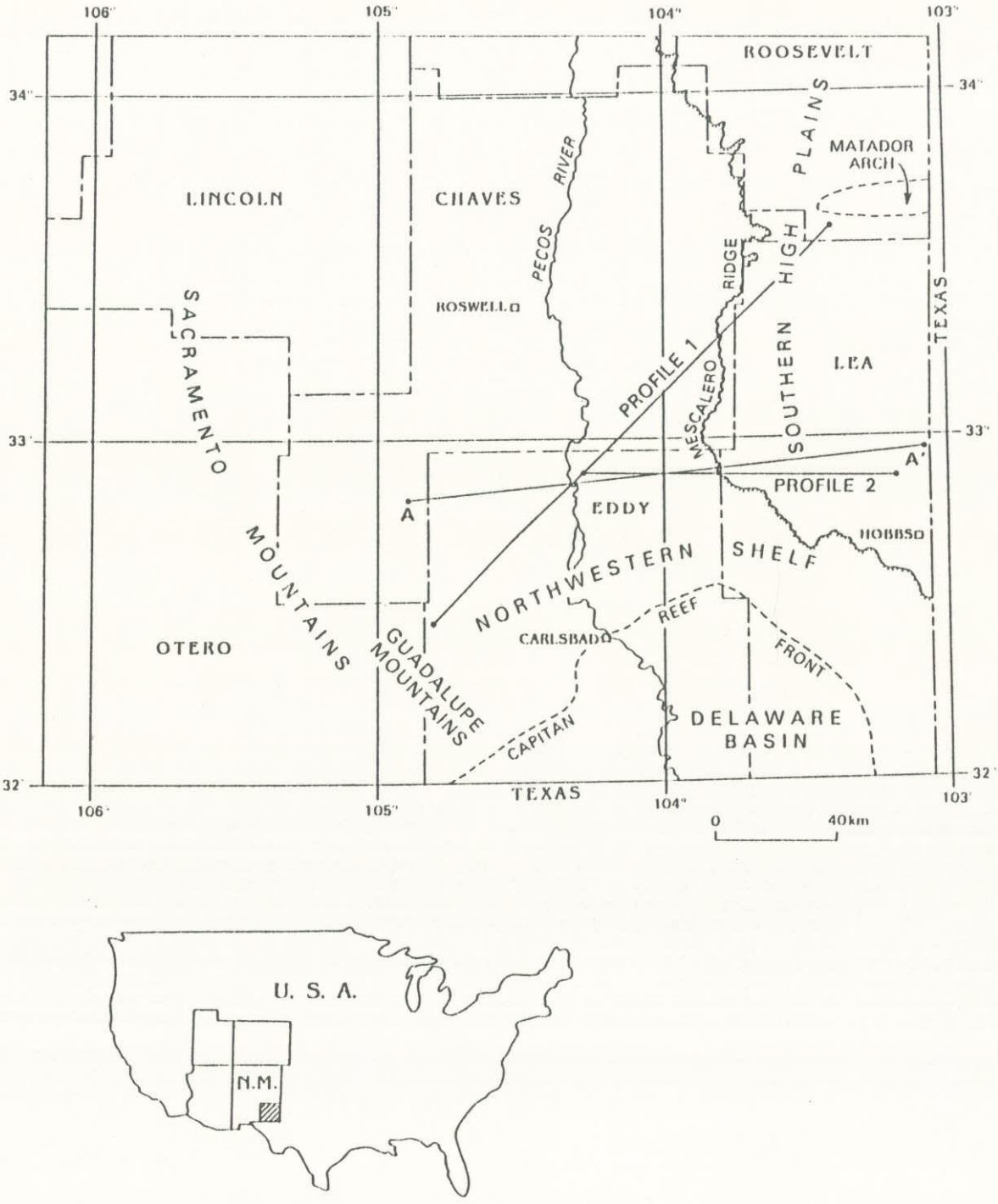

Figure 1. Map of the study area in southeastern New Mexico, showing important regional physiograhic features and locations of profiles.

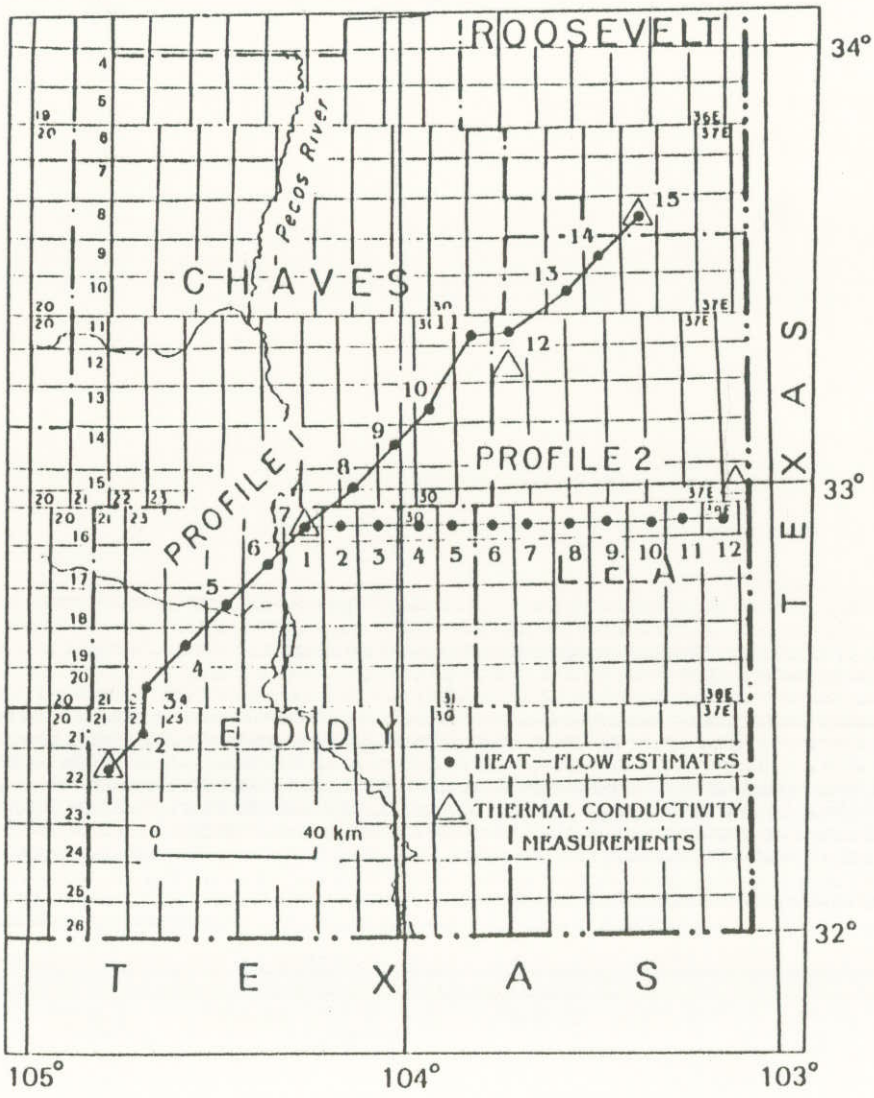

Figure 2. Close-up of the study area showing township and range grid. A single grid block is referred to as a township. Township numbers increase to the south, range numbers increase to the east. Temperature data were averaged over each grid block (township), and gradient values were assigned to the center of the township. Thermal conductivity measurement sites are also shown.

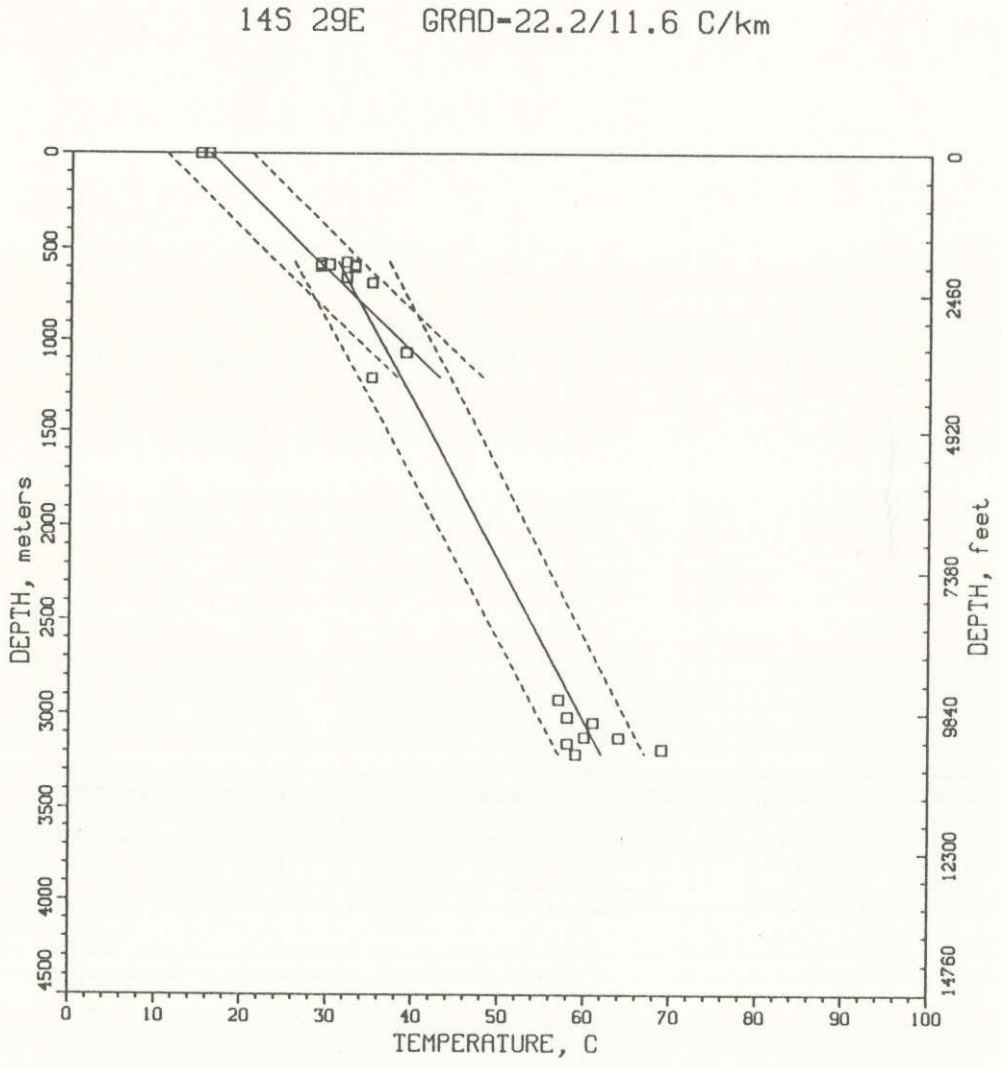

Figure 3. A typical plot of temperature–depth data, with corresponding least mean squares lines fit from surface points to shallow points, and from shallow points to deep points. Dotted lines indicate 95% confidence limits.

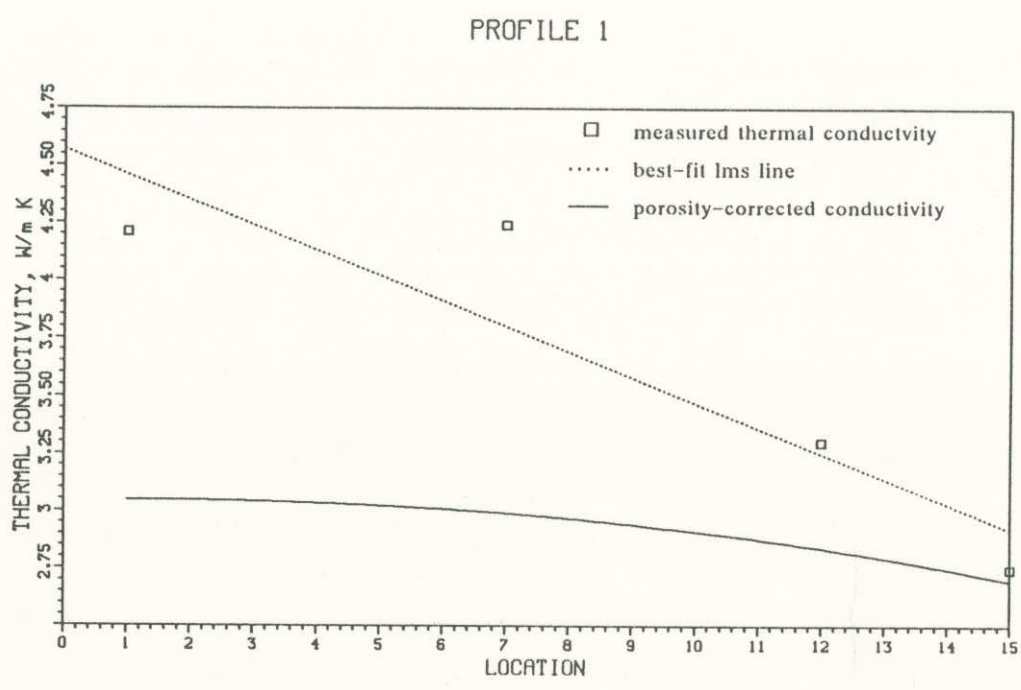

(a)

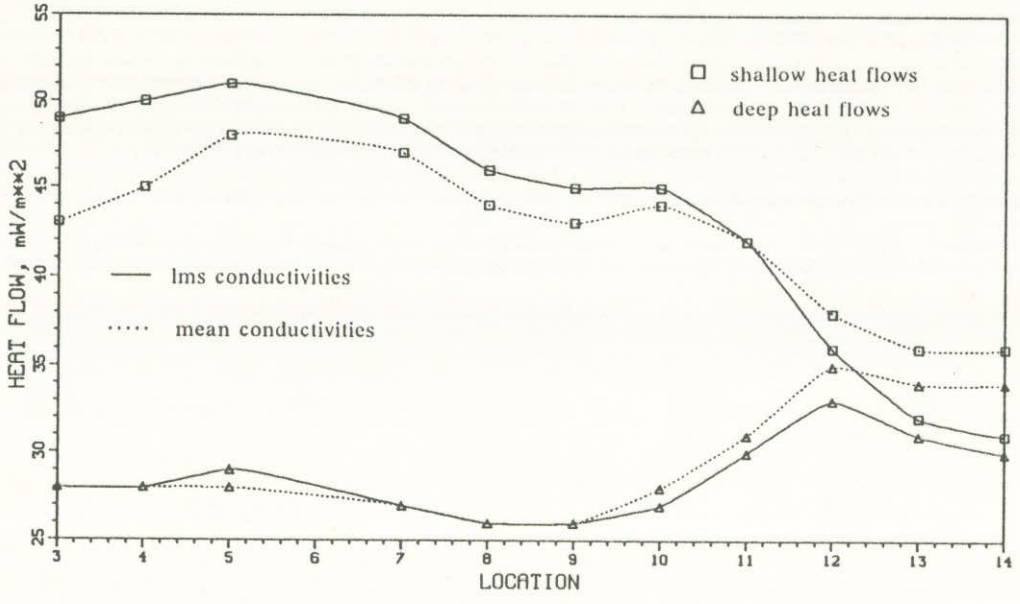

(b)

Figure 4. (a) Comparison of best-fit least mean squares thermal conductivity to porosity-corrected thermal conductivities, assuming a simple linear porosity model (see text). (b) Heat flows along Profile 1 calculated using lms thermal conductivities compared to heat flows calculated using a mean thermal conductivity which remains constant across the basin.

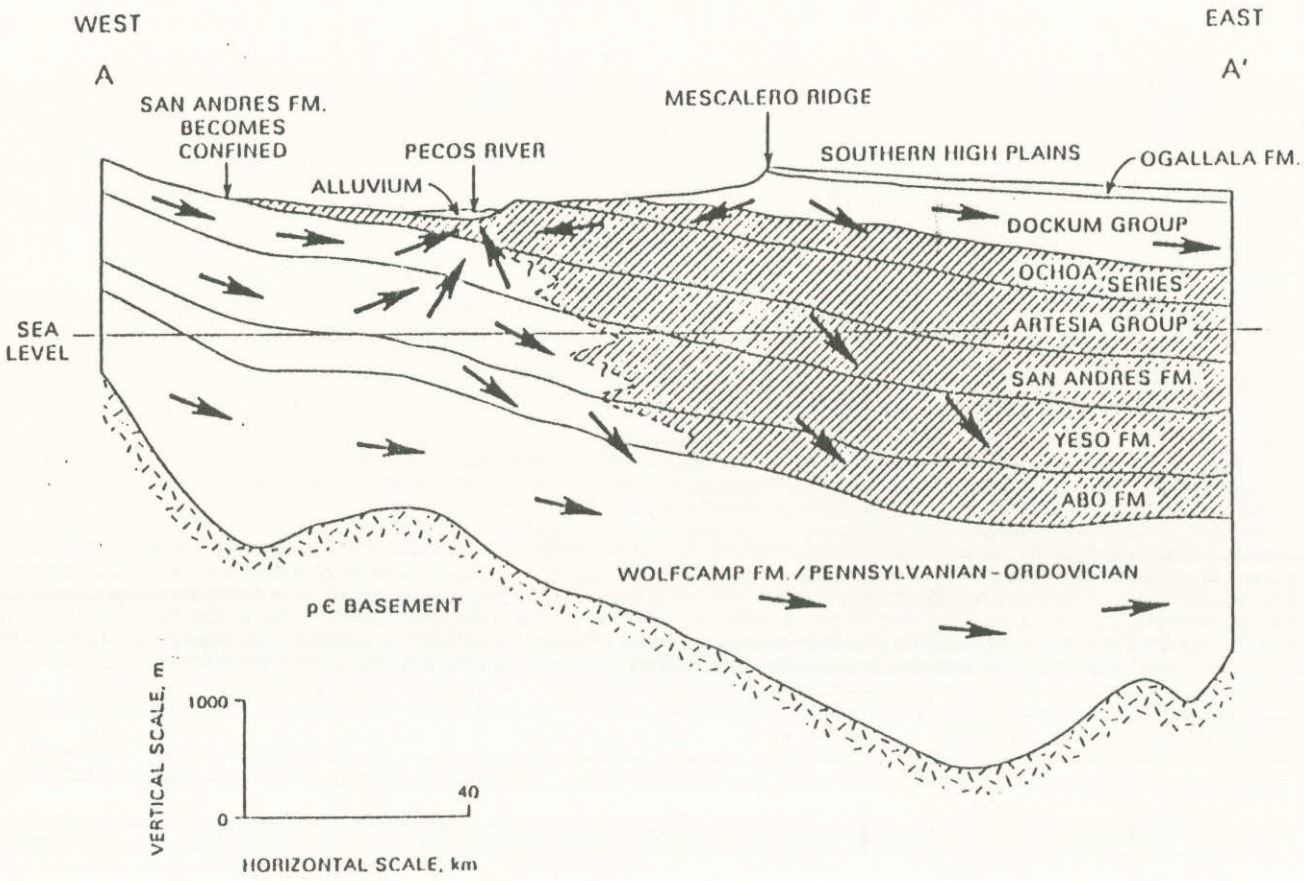

Figure 5. Schematic hydrogeologic cross-section. Flow lines are qualitative and based on the literature, as well as our heat-flow data. The cross-hatched area represents our best guess as to the geometry of the evaporite aquitard.

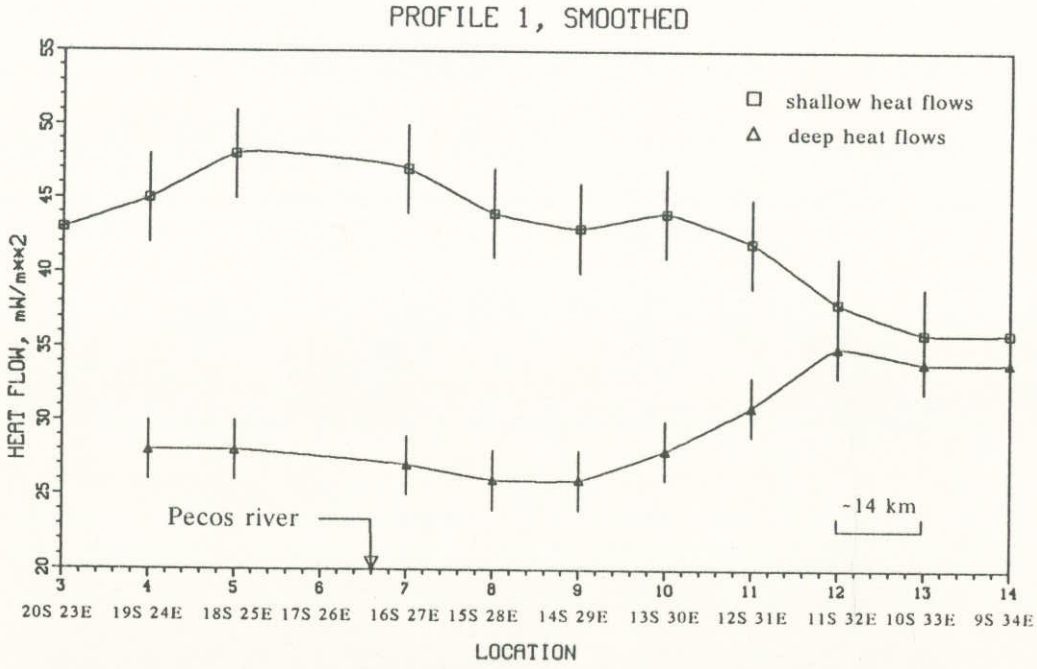

(a)

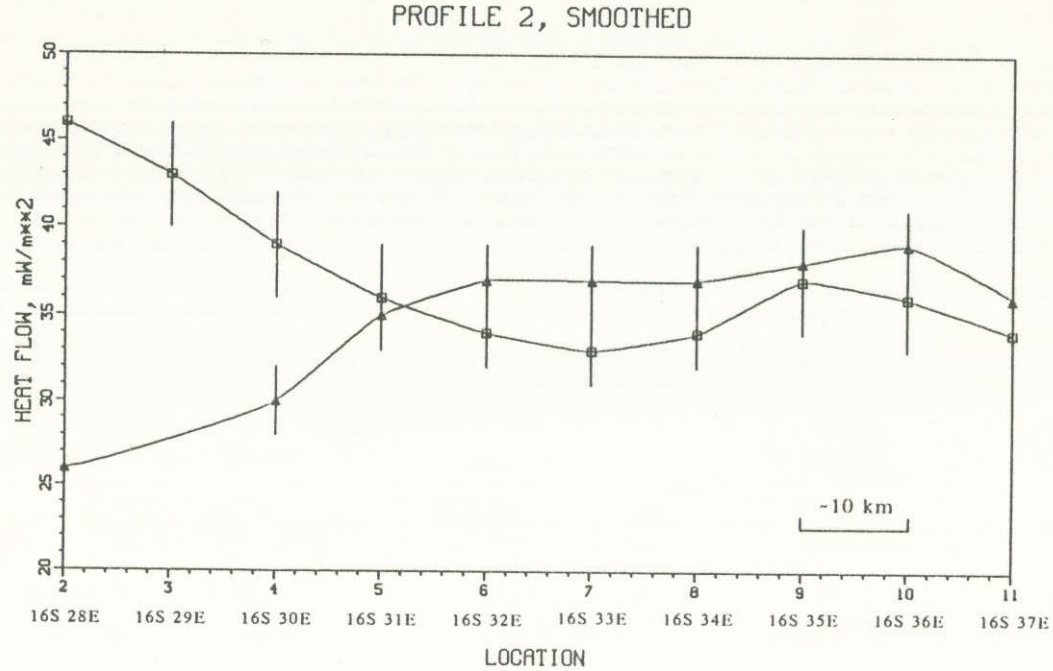

(b)

Figure 6. Three-point average smoothed deep and shallow heat-flow profiles. Error bars are explained in the text. Note that in (b), the Pecos river is located approximately 16 km east of location point two.

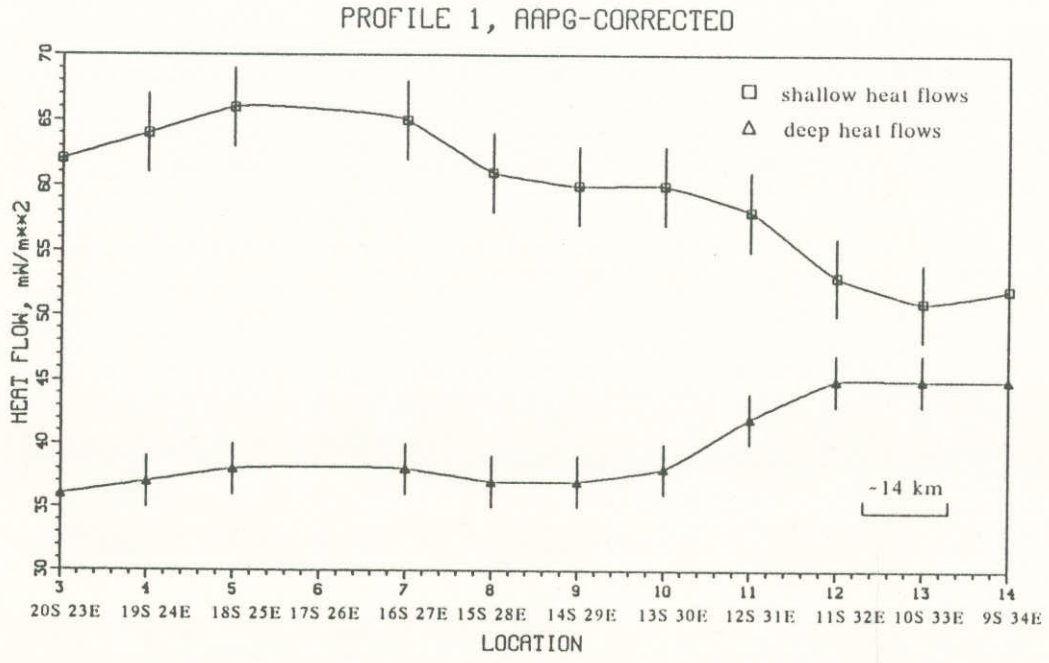

(a)

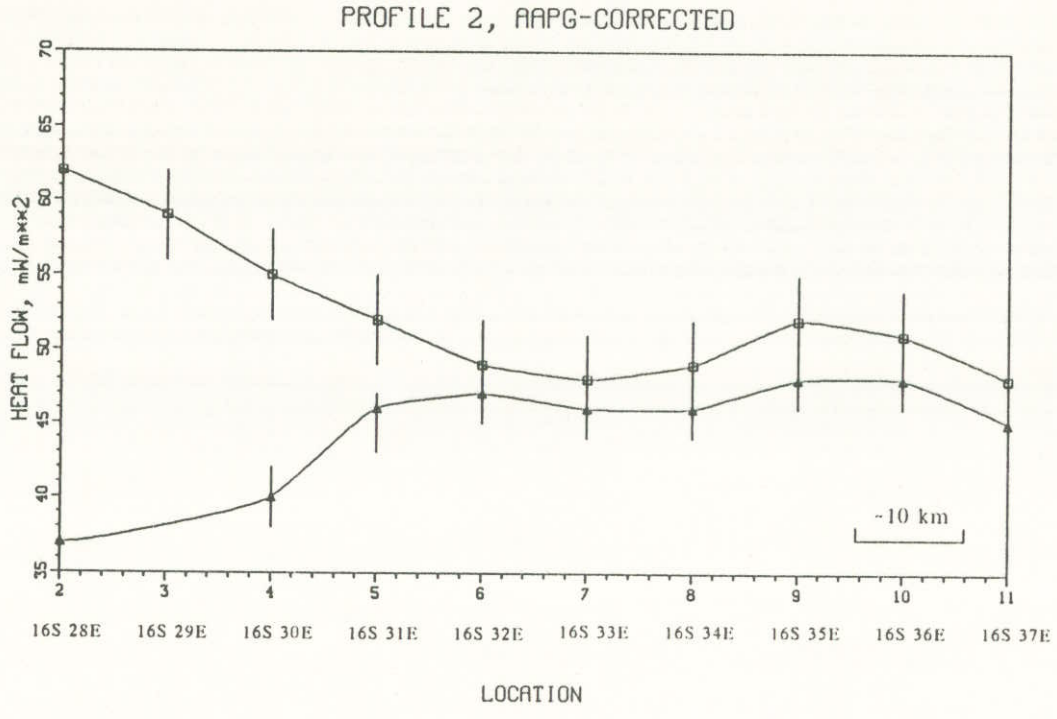

(b)

Figure 7. Three-point average smoothed AAPG-corrected deep and shallow heat-flow profiles. Error bars are explained in the text. Note that in (b), the Pecos river is located approximately 16 km east of location point two.

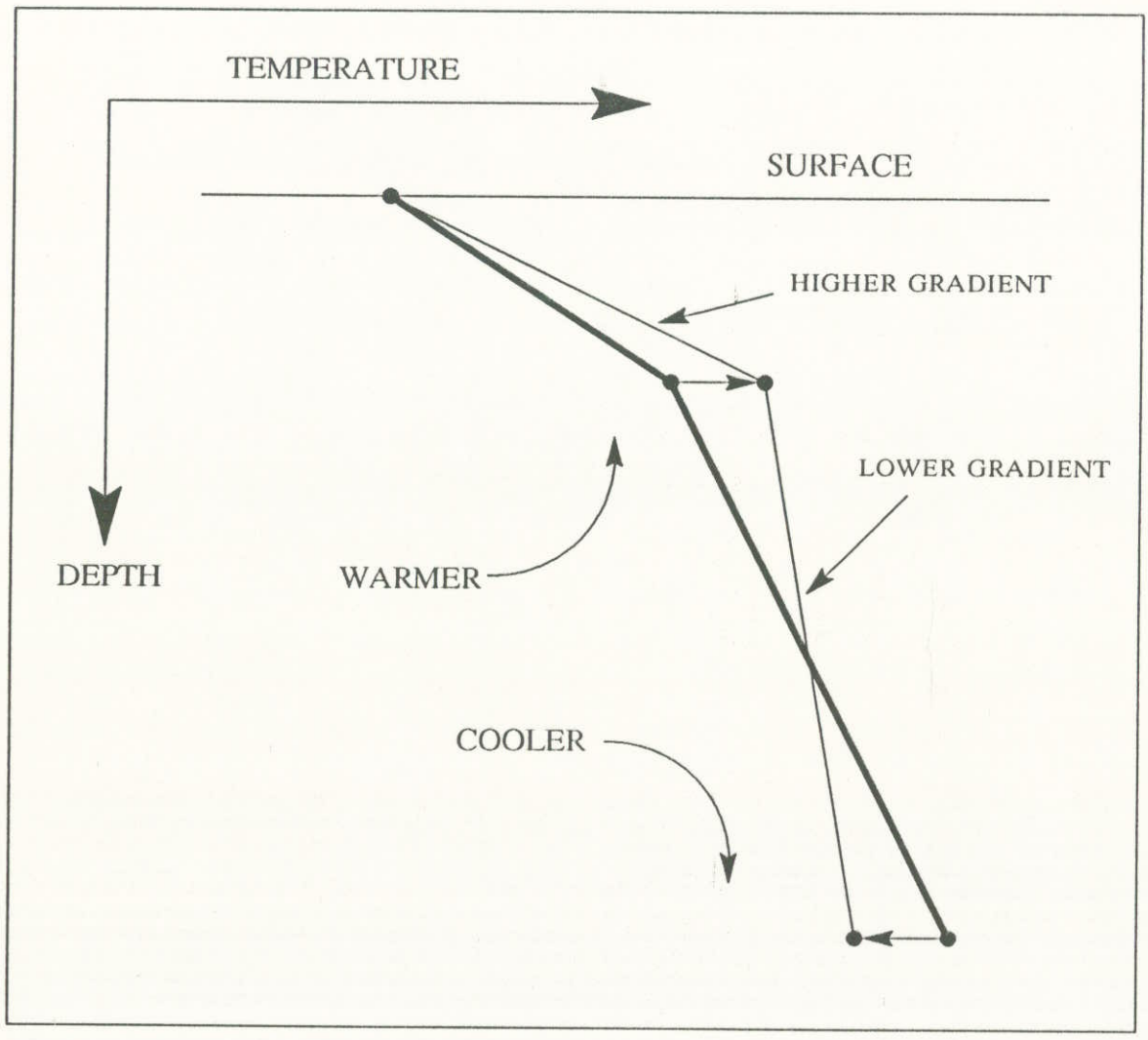

Figure 8. Simple model proposed for increasing shallow heat flows and decreasing deep heat flows by vertical movement of water. Shallow temperatures are increased by upward flow, which lowers shallow temperature gradients and shallow heat flows. Deep temperatures are decreased by downward flow, which decreases deep gradients and heat flows.

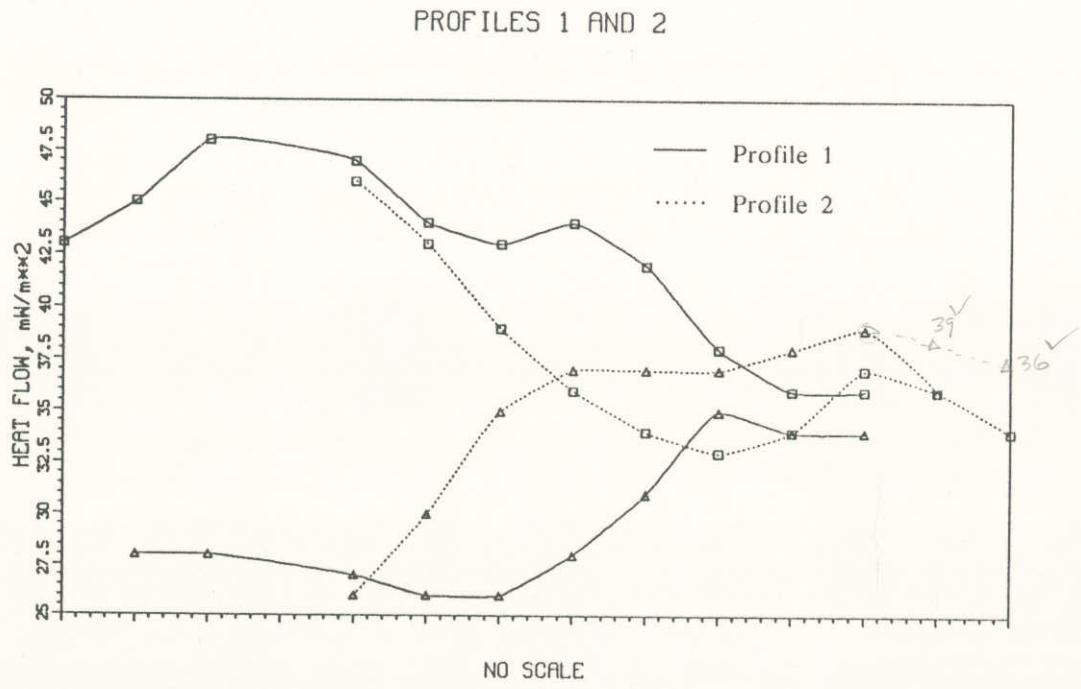

Figure 9. Profile 1 and Profile 2 plotted on the same scale for comparison (uncorrected data). Note that the peaks correspond well, but that Profile 1 is still somewhat broader than Profile 2.

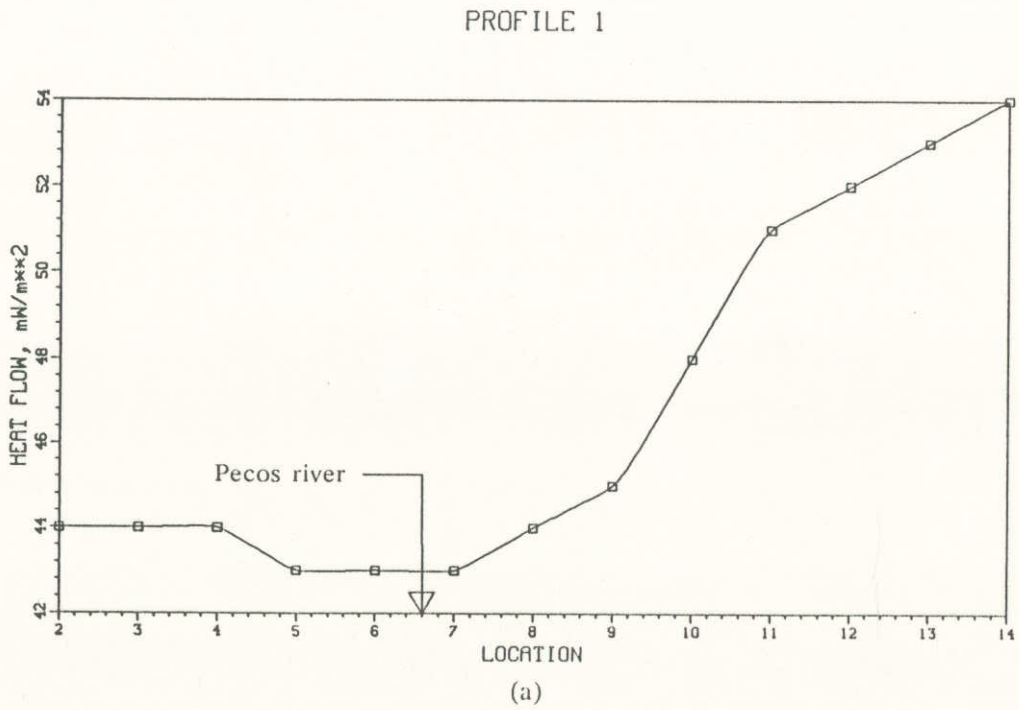

(a)

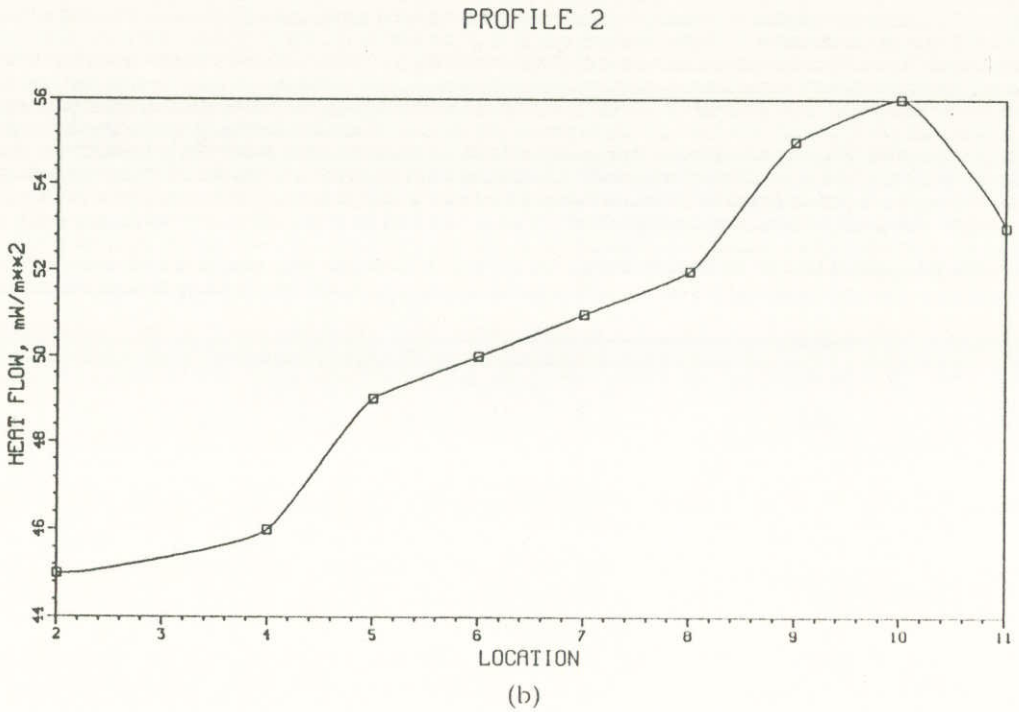

(b)

Figure 10. AAPG-corrected surface-to-deep heat flows along Profile 1 and Profile 2. Surface-to-deep heat flows are measured from surface to deep points. Note that in (b), the Pecos river is approximately 16 km east of location point two.

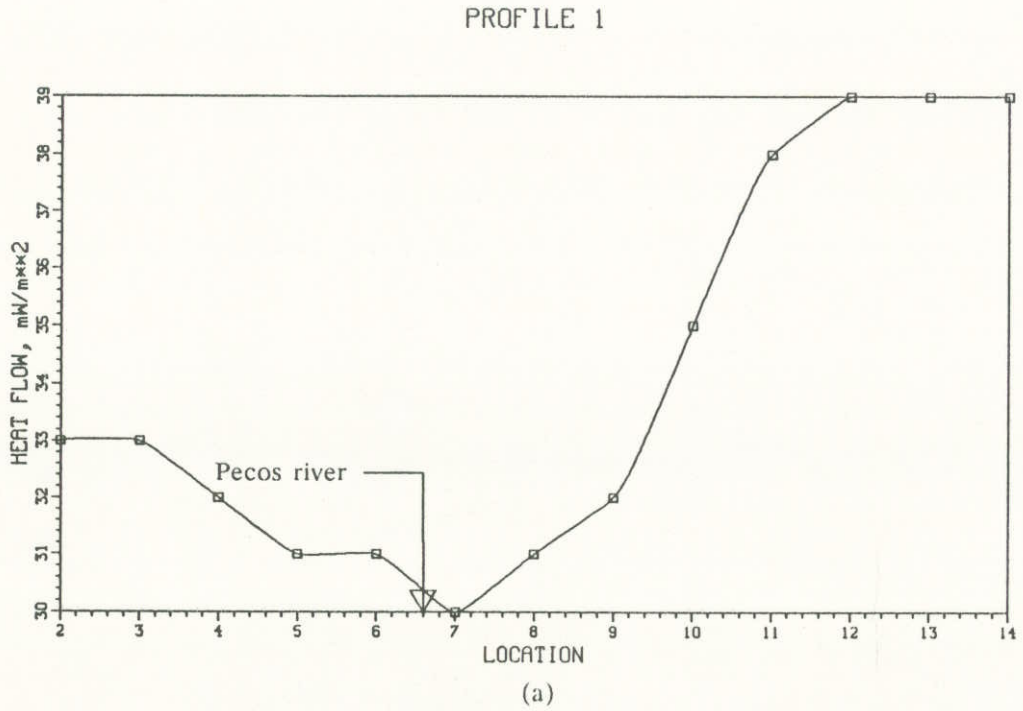

(a)

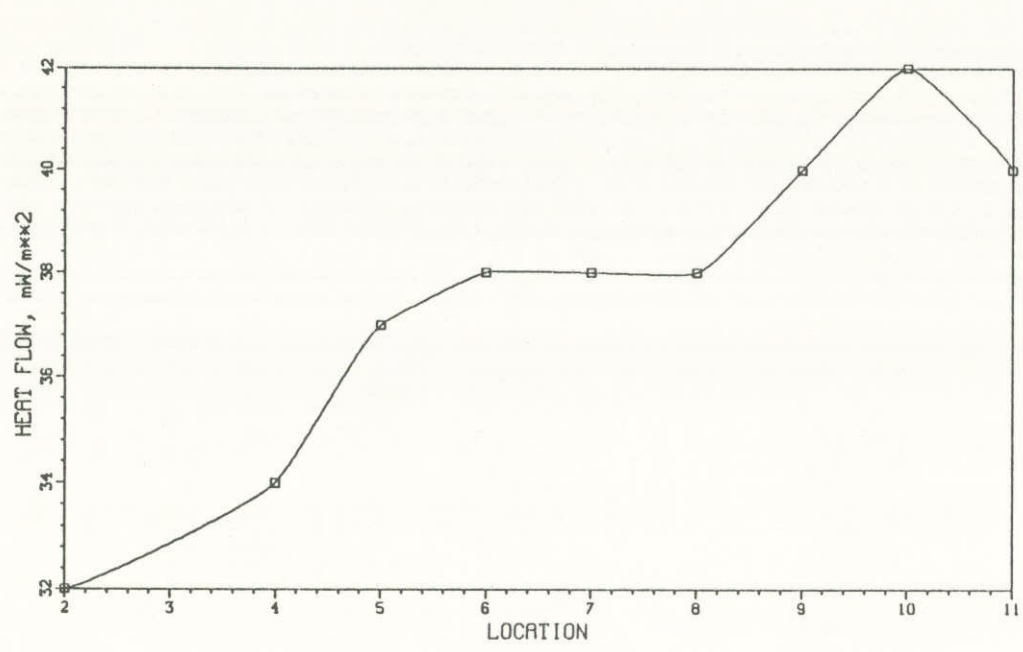

(b)

Figure 11. Uncorrected surface-to-deep heat flows along Profile 1 and Profile 2. Surface-to-deep heat flows are measured from surface to deep points. Note that in (b), the Pecos river is approximately 16 km east of location point two.

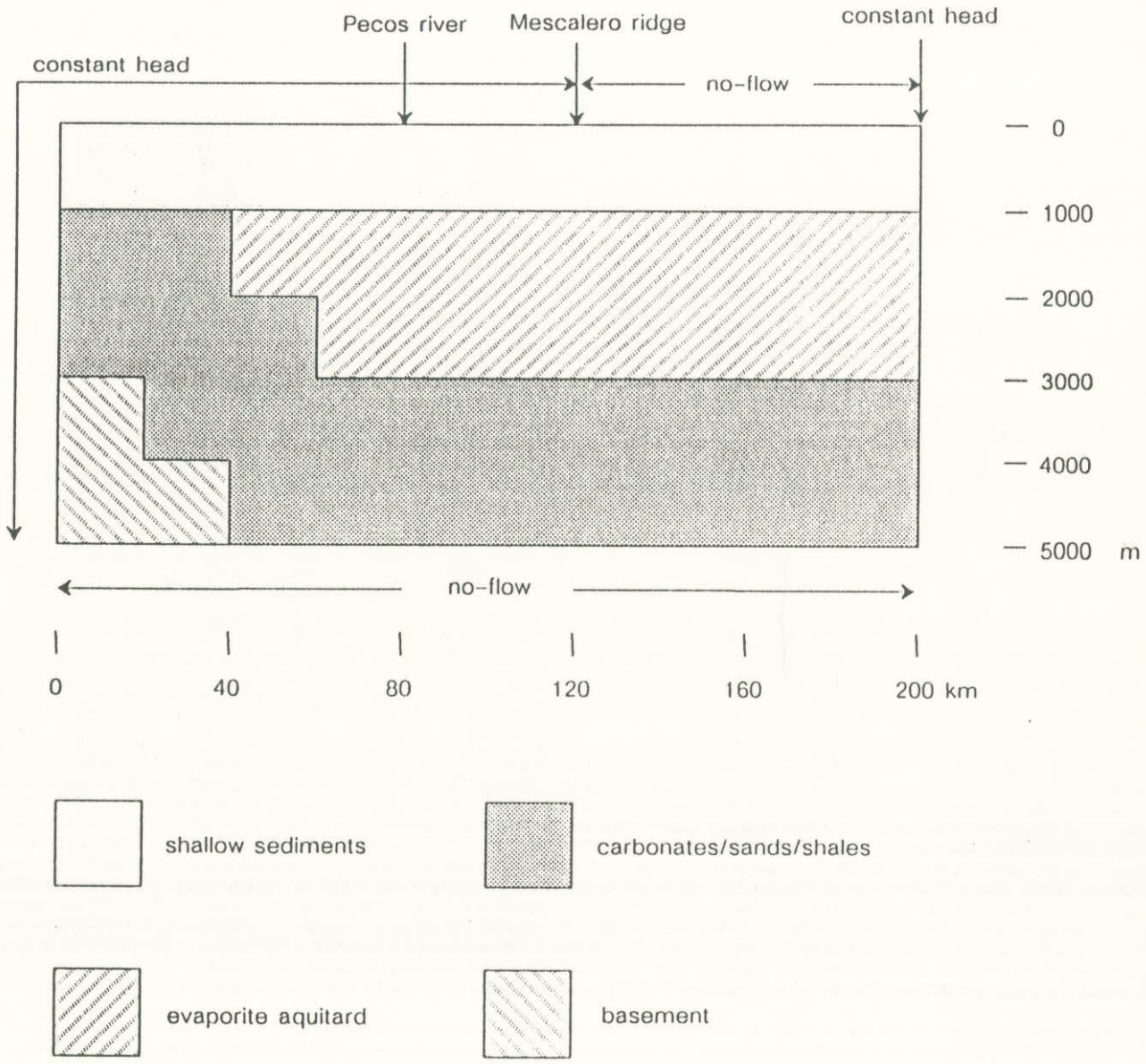

Figure 12. Boundary conditions and hydraulic conductivity distribution of the numerical model. Shallow sediments are representative of the Dockum Group, and the upper portions of the San Andres and the evaporite aquitard (see Figure 5). The lower portion of the evaporite aquitard is characterized by very low hydraulic conductivity. Carbonates, sands, and shales make up the majority of the flow system. Basement rocks are essentially impermeable.

Figure 13. Results from the numerical model. Velocity vectors indicate direction and magnitude of ground-water flow. Shallow and deep heat flows from this scenario are presented. Note the peak in the shallow heat flow which coincides with the Pecos river (at about 80 km).

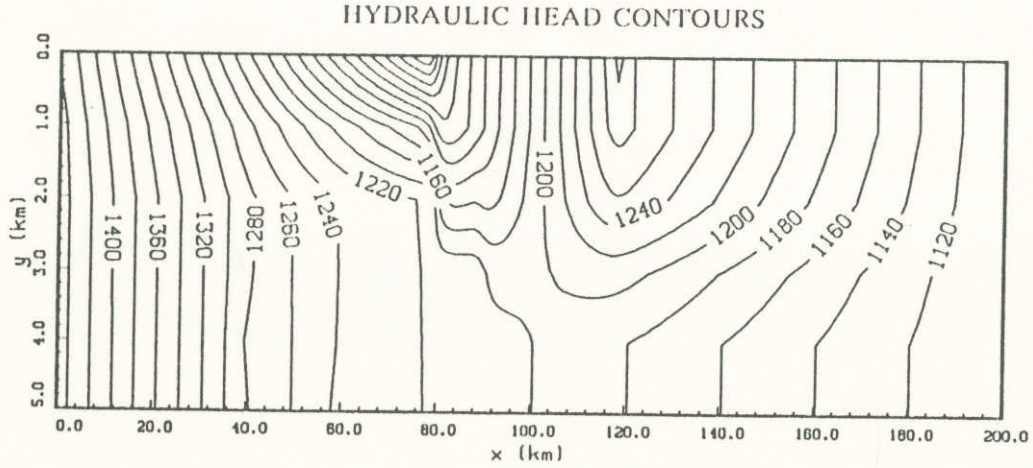

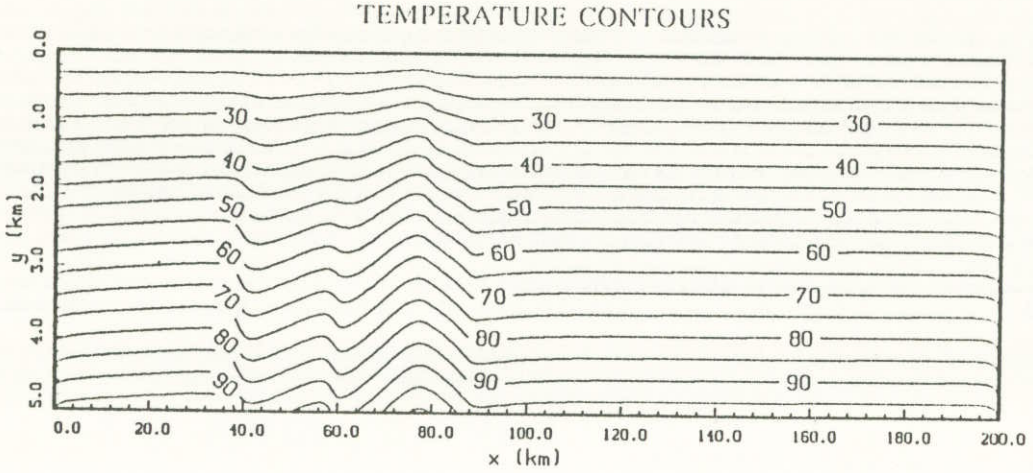

Figure 14. Hydraulic head and temperature contours from the numerical model. Note the elevated temperatures in the area of the Pecos river (at about 80 km).

Table 1. Porosity-corrected harmonic mean thermal conductivities

LOCATION	22S 21E	16S 27E	12S 32E	8S 35E	15S 38E	MEAN (σ)
FORMATION(S)						
post-San Andres	-----	3.01(9)	2.00(9)	2.14(9)	2.14(13)	2.32(0.20)
San Andres	4.21(10)	4.24(3)	3.30(4)	2.75(8)	4.08(4)	3.72(0.26)
Yeso	4.41(7)	4.17(6)	3.60(7)	3.60(7)	4.28(5)	4.01(0.15)
Abo	3.32(4)	2.84(3)	2.14(3)	1.97(2)	3.18(3)	2.69(0.24)
pre-Abo	2.50(13)	2.92(12)	2.43(7)	2.39(4)	2.59(10)	2.57(0.08)
whole well	3.08(34)	3.23(33)	2.49(30)	2.47(30)	2.70(35)	2.79(0.14)

harmonic mean conductivity (no. of measurements)

Table 2. Temperature Gradients and Errors, Profile 1

LOCATION	SHALLOW GRAD (σ)	DEEP GRAD (σ)
22S 21E	17.0 (1.78) °C/km	16.7 (2.27) °C/km
21S 22E	-----	-----
20S 23E	19.5 (---)	14.5 (2.73)
19S 24E	15.7 (0.28)	19.5 (1.22)
18S 25E	16.8 (0.29)	15.7 (0.94)
17S 26E	-----	-----
16S 27E	25.9 (3.48)	12.2 (0.87)
15S 28E	17.1 (0.82)	13.9 (0.44)
14S 29E	22.2 (1.45)	11.6 (0.53)
13S 30E	22.2 (1.11)	11.8 (0.58)
11S 31E	22.0 (---)	13.8 (0.44)
11S 32E	19.6 (2.48)	14.2 (0.94)
10S 33E	15.8 (2.21)	14.0 (1.03)
9S 34E	19.4 (0.72)	11.9 (1.17)
8S 35E	18.3 (0.47)	12.5 (0.77)

Table 3. Temperature Gradients and Errors, Profile 2

LOCATION	SHALLOW GRAD (σ)	DEEP GRAD (σ)
16S 27E	25.9 (3.48) °C/km	12.2 (0.87) °C/km
16S 28E	26.4 (3.08)	11.3 (0.77)
16S 29E	21.1 (0.61)	-----
16S 30E	18.5 (0.57)	13.0 (0.49)
16S 31E	17.5 (0.39)	14.4 (0.81)
16S 32E	17.8 (0.96)	15.2 (0.74)
16S 33E	15.5 (0.40)	13.2 (0.80)
16S 34E	17.1 (0.46)	12.5 (0.70)
16S 35E	18.7 (0.70)	14.4 (0.76)
16S 36E	19.6 (2.69)	14.3 (1.03)
16S 37E	15.5 (1.38)	14.1 (0.63)
16S 38E	15.8 (0.58)	13.0 (0.73)

Table 4. AAPG-Corrected Heat Flows and Errors, Profile 1

LOCATION	SHALLOW HEAT FLOW (σ)	DEEP HEAT FLOW (σ)
22S 21E	65 (2.7) mW/m²	36 (2.4) mW/m²
21S 22E	-----	-----
20S 23E	58 (3.0)	32 (2.2)
19S 24E	62 (2.6)	41 (2.7)
18S 25E	71 (3.0)	38 (2.3)
17S 26E	-----	-----
16S 27E	66 (3.8)	36 (2.0)
15S 28E	57 (2.7)	39 (2.1)
14S 29E	59 (3.3)	36 (1.9)
13S 30E	63 (3.3)	37 (1.8)
11S 31E	59 (3.3)	42 (2.0)
11S 32E	51 (3.0)	46 (2.1)
10S 33E	49 (2.6)	47 (2.0)
9S 34E	52 (3.0)	43 (1.8)
8S 35E	54 (2.8)	46 (1.9)

Table 5. AAPG-Corrected Heat Flows and Errors, Profile 2

LOCATION	SHALLOW HEAT FLOW (σ)	DEEP HEAT FLOW (σ)
16S 27E	65 (3.8) mW/m²	36 (2.0) mW/m²
16S 28E	61 (3.8)	35 (1.9)
16S 29E	61 (3.2)	-----
16S 30E	54 (2.9)	41 (2.0)
16S 31E	51 (2.8)	44 (2.0)
16S 32E	50 (2.8)	49 (2.0)
16S 33E	46 (2.5)	43 (1.8)
16S 34E	49 (2.7)	45 (1.8)
16S 35E	53 (2.9)	50 (1.9)
16S 36E	54 (3.0)	48 (2.0)
16S 37E	45 (2.5)	46 (1.9)
16S 38E	46 (2.6)	42 (1.8)

Table 6. Heat Flows and Errors, Profile 1

LOCATION	SHALLOW HEAT FLOW (σ)	DEEP HEAT FLOW (σ)
22S 21E	45 (2.4) mW/m²	28 (2.4) mW/m²
21S 22E	-----	-----
20S 23E	41 (2.7)	23 (2.1)
19S 24E	42 (2.2)	32 (2.7)
18S 25E	51 (2.7)	28 (2.2)
17S 26E	-----	-----
16S 27E	50 (3.6)	24 (1.7)
15S 28E	39 (2.4)	28 (1.9)
14S 29E	44 (3.1)	25 (1.6)
13S 30E	46 (3.1)	26 (1.7)
11S 31E	43 (3.1)	33 (1.9)
11S 32E	37 (2.8)	35 (2.0)
10S 33E	33 (2.2)	37 (2.0)
9S 34E	38 (2.7)	31 (1.7)
8S 35E	38 (2.6)	34 (1.8)

Table 7. Heat Flows and Errors, Profile 2

LOCATION	SHALLOW HEAT FLOW (σ)	DEEP HEAT FLOW (σ)
16S 27E	49 (3.6) mW/m²	25 (1.7) mW/m²
16S 28E	46 (3.7)	23 (1.6)
16S 29E	44 (3.0)	-----
16S 30E	38 (2.6)	30 (1.8)
16S 31E	35 (2.4)	36 (2.0)
16S 32E	35 (2.5)	40 (2.1)
16S 33E	31 (2.2)	35 (1.9)
16S 34E	34 (2.4)	35 (1.8)
16S 35E	37 (2.6)	41 (2.0)
16S 36E	39 (2.8)	38 (2.0)
16S 37E	31 (2.2)	37 (2.0)
16S 38E	31 (2.2)	34 (1.8)